CHALMERS
UNIVERSITY OF TECHNOLOGY

A material degradation study of novel FeCrAl alloys, stainless steels and nickel base alloy in fluidized bed heat exchangers of a waste-fired CFB

Downloaded from: https://research.chalmers.se, 2024-05-05 02:50 UTC

Citation for the original published paper (version of record):
Lindmark, H., Phother Simon, J., Olausson, M. et al (2023). A material degradation study of novel FeCrAl alloys, stainless steels and nickel base alloy in
fluidized bed heat exchangers of a waste-fired CFB boiler. Fuel, 338.
http://dx.doi.org/10.1016/j.fuel.2022.127299

N.B. When citing this work, cite the original published paper.

research.chalmers.se offers the possibility of retrieving research publications produced at Chalmers University of Technology.
It covers all kind of research output: articles, dissertations, conference papers, reports etc. since 2004.
research.chalmers.se is administrated and maintained by Chalmers Library

(article starts on next page)

Fuel 338 (2023) 127299

Contents lists available at ScienceDirect

Fuel

journal homepage: www.elsevier.com/locate/fuel

A material degradation study of novel FeCrAl alloys, stainless steels and nickel base alloy in fluidized bed heat exchangers of a waste-fired CFB boiler

Hampus Lindmark [a,*], Julien Phother [a], Maria Dolores Paz Olausson [a], Johanna Nockert [b], Fredrik Lind [c], Anna Jonasson [c], Vesna Barišić [d], Kyösti Vänskä [d], Laura Rioja-Monllor [e], Jesper Liske [a]

[a] Energy and Materials, Department of Chemistry and Chemical Engineering, Chalmers University of Technology, SE412 96, Gothenburg, Sweden
[b] Kanthal AB, SE734 27, Hallstahammar, Sweden
[c] E.On Energy Infrastructure AB, SE205 09 Malmö, Sweden
[d] Sumitomo SHI FW, FI782 01 Varkaus, Finland
[e] Alleima AB, SE811 81 Sandviken, Sweden

ARTICLE INFO

Keywords:
Waste-fired boiler
Loop seal
High-temperature corrosion
FeCrAl alloys
Austenitic alloys
Ni-base alloy

ABSTRACT

This study aimed to evaluate the material degradation resistance of two newly developed FeCrAl alloys exposed within the loop seal region of an 85 MW_{th} waste-fired CFB boiler in Sweden. In addition to the FeCrAl alloys, two commercial austenitic stainless steel and one nickel base (Ni-base) alloy were also studied. The samples were exposed for 6 and 12 months by clamping half-moon rings onto tubes of the installed superheater bundle, achieving a material temperature of 500–520 °C. The material degradation of the samples was assessed by evaluating material loss using an ultrasonic thickness gauge in combination with a scanning electron microscope (SEM). Microstructural analysis was carried out using SEM coupled with Energy-dispersive X-ray spectroscopy (EDX).

Both FeCrAl alloys showed promising results achieving material losses in the same range as the investigated austenitic stainless steels and the Ni-base alloy. A thin inward-growing Cr/Al-rich and thick outward-growing Fe-rich oxide were present for the FeCrAl alloys, and an internal nitridation zone was formed in the material matrix close to the metal/oxide interphase. The material loss and extent of the corrosion attack for the austenitic stainless steels varied depending on the alloy composition. However, the corrosion attack remained similar, as all the austenitic steels suffered from internal and intergranular corrosion. For the Ni-base alloy, the attack was defined by an internal Cr-rich oxide formation with no intergranular corrosion.

This study suggests that the novel FeCrAl alloys provide satisfying resistance towards corrosion and erosion of the fluidized bed heat exchangers in the loop seal region of a waste-fired boiler. In addition, the stainless steel SX and the Ni-base alloy Sanicro® 69 performed well. Furthermore, the results revealed that corrosion rather than erosion was the dominating degradation process of the investigated samples, as deposit formation was observed on most of the samples as well as corrosion product layers. Thus, the erosive aspect of the attack was expected to be minor.

1. Introduction

Sustainable fuels, such as residual biomass and waste, have during the last decades outcompeted fossil coal as the preferred fuel for combined heat and power production plants (CHP) in Nordic countries as an approach to reduce the net release of CO_2 emission to the atmosphere [1–4].

The major drawback with the combustion of biomass and waste is the presence of corrosive components in the flue gas, such as, e.g., alkali and chlorine-containing chemical species. Some of these flue gas components condense on superheaters situated in the convective pass of the boiler and form a deposit on the heat transfer surfaces. Such deposit

* Corresponding author.
E-mail address: lhampus@chalmers.se (H. Lindmark).

https://doi.org/10.1016/j.fuel.2022.127299
Received 11 October 2022; Received in revised form 8 December 2022; Accepted 24 December 2022
Available online 4 January 2023
0016-2361/© 2023 The Authors. Published by Elsevier Ltd. This is an open access article under the CC BY license (http://creativecommons.org/licenses/by/4.0/).

layers have been shown to severely increase the corrosion rate and reduce the heat transfer efficiency of the superheaters [5–13].

The Circulating Fluidized Bed technology (CFB) has been recognized for its high environmental performance and fuel flexibility for large-scale combustion of biomass and waste fuels. In an effort to increase the efficiency of CHP based on the CFB technology, superheating of the steam in the loop seal area of the CFB hot loop has been developed. This region is interesting from a superheater point of view as it provides high heat transfer properties from the hot bed material (which consists of a mixture of sand and ashes) as well as a less corrosive environment compared to the corresponding, more traditional location in the convective pass. Having superheater tubes submerged in a bed of solids may, on the other hand, increase the risk of localized erosion. In addition, corrosive species can be transported into this region by the circulated bed material and condense on the superheater tubes. This may lead to an increased degradation rate due to the synergetic effect of erosion and corrosion [14–16].

One approach to mitigate the degradation rate of superheaters in this application is to introduce high-performance materials. Austenitic stainless steels are commonly used in this application for their ability to form a protective and dense chromium-rich (Cr-rich) oxide in a wide temperature range and environments. Nevertheless, the primary chromium oxide in waste-fired boilers will eventually break down and form a less protective iron-rich (Fe-rich) oxide due to the corrosive environment leading to extensive material loss. However, the corrosion resistance can be further improved by introducing nickel base (Ni-base) alloys to the superheaters, which is also associated with a higher material cost [14]. Thus, there is room for improvement regarding material selection to enhance electrical efficiency in waste-fired boilers.

FeCrAl alloys are traditionally acclaimed for their excellent resistance to corrosion at temperatures ranging from 900 to 1300 °C due to their ability to form α-Al_2O_3. This form of alumina is thermodynamically stable, achieving a high degree of stoichiometry with good protective properties towards water and alkali chloride-induced corrosion [17–18]. At temperatures below 900 °C, transient γ-Al_2O_3 is usually formed, which has less corrosive protective properties than its thermodynamically stable form [19]. Lab-scale studies have shown that the corrosion protection of FeCrAl alloys is significantly improved with the addition of Si in aggressive corrosive environments [20–22]. Similar tests were conducted in field exposures showing that silicon-containing FeCrAl alloys with > 10 wt% chromium showed comparable corrosion resistance to that of a Ni-base alloy (Alloy 625) [8]. The mentioned study was conducted in the conventional convective pass of a biomass-fired boiler that is known to have a higher concentration of aggressive corrosive species than the corresponding region in the loop seal. Implementation of FeCrAl alloys as a coating material on superheater tubes in the loop seal region of a full-scale CFB plant has been studied by Nafari et al. Here, the FeCrAl material, Kanthal A1, was exposed for two years using 100 % wood (logging residues) as fuel at material temperatures of 510–550 °C. The results suggest that the Kanthal A1 coating performed well without any sign of delamination or cracks after two years of exposure [14]. However, as the fuel composition in the aforementioned study give rise to a mildly corrosive environment, it is of importance to further study FeCrAl alloys in different environments to properly ascertain its protective properties for the present application.

The aim of this study was to evaluate the performance of two novel FeCrAl materials, Kanthal® EF100 and Kanthal® EF101, exposed within the loop seal region of an 85 MW_{th} waste-fired CFB boiler in Sweden. In addition, two commercialized austenitic stainless steel and one Ni-base alloy were exposed simultaneously. The samples were exposed for 6 and 12 months by clamping half-moon rings onto tubes of the installed superheater tube bundle, achieving a material temperature of 500–520 °C. The material performance was evaluated by comparing material loss data and oxide microstructure between the samples using an ultrasonic thickness gauge in combination with SEM. Microstructural analysis was carried out using SEM/EDX.

2. Experimental

2.1. Material matrix and sample preparation

In this study, five materials have been investigated, the austenitic stainless steels 316Ti and Alleima® SX, the austenitic Ni-base alloy Sanicro® 69 (San69), and two ferritic FeCrAl alloys Kanthal® EF100 and Kanthal® EF101. The chemical composition of the five studied alloys is presented in Table 1. Kanthal® EF100 and EF101 have been developed to increase the temperature interval where FeCrAl alloys are normally used down to temperatures as low as 300 °C. By lowering the Cr content to about 10 wt%, the α-α' phase separation, caused by a miscibility gap in the Fe-Cr system, is avoided. This α-α' phase separation is also known as 475 °C embrittlement, and when suppressed, the alloys see a significant improvement in the mechanical properties at these lower temperatures. In addition, the two FeCrAl alloys contain additional alloying elements such as manganese (Mn) reactive elements (RE) and silicon (Si), where the latter element is added to improve the ability to form a protective oxide scale at intermediate temperature as previously reported in [21].

Two half-moon sample rings were prepared for each material and subsequently mounted on the top- and bottom-most rows of the fluidized bed heat exchanger (FBHE) tube bundle during boiler shutdown using TIG-welding with Alloy 625 wire. The two half-moon samples were characterized as a wind-side sample (facing down towards the loop seal air nozzles) and a lee-side sample (facing up towards the return leg of the cyclone). In this study, the wind-side samples (facing down) have been investigated. The installed clamps can be seen in the bottom left picture in Fig. 1.

2.2. Exposure

The tested materials were exposed to an 85 MW_{th} Waste-to-Energy CFB boiler owned and operated by E.ON Energy Infrastructure AB in Sweden. The boiler has been in continuous operation since 2010. The boiler produces steam, primarily used for the production of electricity, industrial process steam, and district heating, and is in operation for roughly 7000 h annually, including two planned maintenance stops. A summary of the supplied fuel mix is presented in Fig. 1 to the right. The fuel is a mix of primary industrial waste and household waste, which is sorted and pretreated before combustion. The circulating bed material includes roughly 30 wt% natural silica sand and 70 wt% of fuel ashes. Superheating of the steam to 450 °C (65 bar) is carried out through a series of superheaters, and the final steam temperature is controlled by injections of feed water before and after the first FBHE superheater. Material surface temperatures were estimated by using a boiler design software alongside with the measured steam temperatures. From these measurements, it was concluded that a material temperature of roughly 500–520 °C was achieved. The air velocity in the FBHE chamber was around 0.4 m/s. The exposure lasted for 6 and 12 months.

2.3. Analysis

The exposed clamps were dismounted using an angle grinder on the weld. Subsequently, the half-moon clamps were cast in epoxy and cut with an automatic saw to obtain a cross-section. The cross-section was ground and polished using SiC paper down to 4000 grit. A thin gold film of roughly 40 nm was sputtered onto the samples to increase conductivity and imaging contrast. Microstructure and material loss measurements were performed using SEM (FEI QUANTA 200 FEG ESEM) with backscattered electrons (BSE) detector operating in high vacuum mode and running at an accelerated electron voltage of 15–20 keV. The instrument was coupled with an Oxford Instruments X-MAX 80 energy dispersive X-ray (EDX) detector for analysis of elemental mapping and chemical quantification. The material loss was evaluated by measuring the material thickness at three different positions on the half-moon

Table 1
Chemical composition (wt%) of tested alloys in increasing Cr and Ni content.

Material	Wt%								
	Fe	Cr	Al	Ni	Mn	Si	Mo	Cu	Minor elements
Kanthal®EF100	Bal.	10.1	4.0	x	<0.2	0.3	x	x	C, RE*
Kanthal®EF101	Bal.	12.4	3.7	x	<0.1	1.3	x	x	C, RE*
316Ti	Bal.	16.5	x	11	2.0	0.8	2.1	x	C, S, P, Ti
SX	Bal.	17.5	x	19.5	0.5	5.0	0.4	2.0	C, S, P
San69	10	30	x	60	<0.5	<0.5	x	x	C, S, P

* Reactive elements.

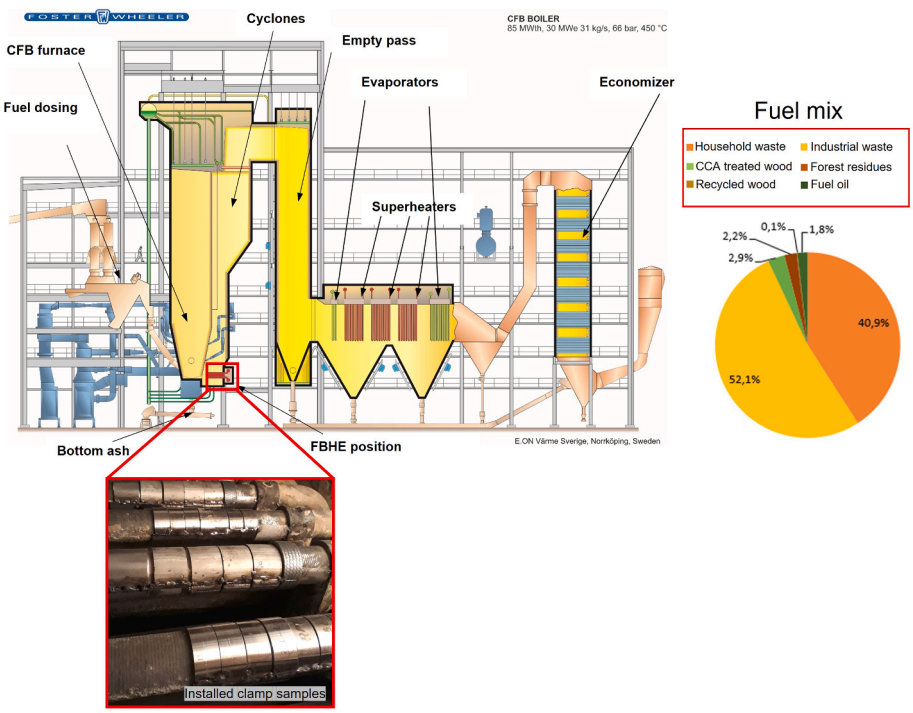

Fig. 1. Clamps mounted onto the superheater tubes (below), a schematic picture of the boiler, and a summary of the supplied fuel (right) .

clamp before exposure using an Olympus 27MG ultrasonic thickness gauge with a 0.01 mm resolution. The thickness was measured post-exposure at nine locations in similar positions as before exposure using the SEM setup mentioned above. The thickness measurements did not include regions of internal oxidation nor nitridation zones as material loss.

3. Results

3.1. Material loss

A summary of the results of material losses after 6 and 12 months of exposure is shown in Fig. 2. Material loss data of San69 and EF101 after 12 months of exposure could not be retrieved. A general trend was observed, showing that the material loss increased as a function of exposure time. After 12 months of exposure, 316Ti exhibited the highest measured material loss (1.15 mm/year). The FeCrAl alloy EF100 outperformed 316Ti after 12 months of exposure, obtaining a material loss of 0.19 mm/year, which was similar to SX (0.22 mm/year). Although material losses for 12 months could not be retrieved for San69 and EF101, they exhibited significantly low material losses after 6 months, roughly 0.08 mm and 0.1 mm, respectively.

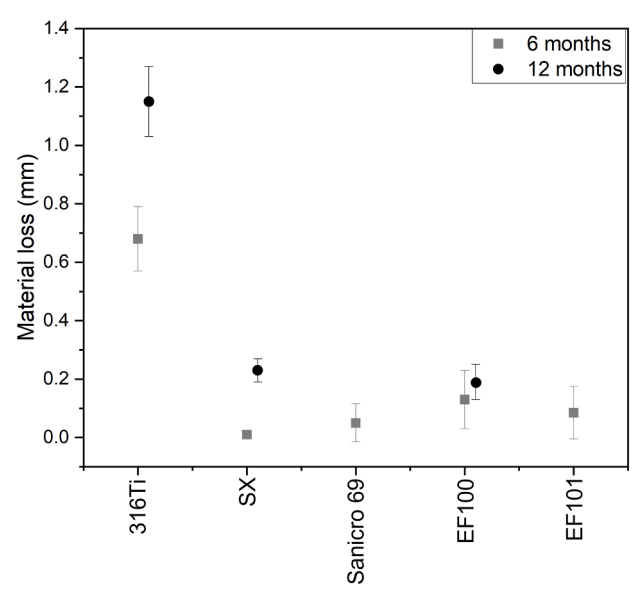

Fig. 2. Material losses after 6 and 12 months of exposure.

3.2. Microstructure analysis

3.2.1. Austenitic stainless steels

The cross-section images after 6 and 12 months of exposure for 316Ti are shown in Fig. 3a and c. Similar features were observed for both samples, and thus, chemical analysis via EDX mapping is only shown for the sample exposed for 12 months. For 316Ti, the cross-section showed little or no deposit layer as well as a minor indication of the formation of an outer corrosion product layer. Instead, the cross-sections revealed signs of intergranular corrosion attacks (see Fig. 3b and 3d). Compared to the FeCrAl alloys, the material loss was considerably higher, as the 6-month 316Ti sample exhibited a material loss roughly 7 times higher than the FeCrAl alloys (see Fig. 2).

Fig. 3e shows the EDX mapping of 316Ti exposed for 12 months. A thin outer layer of oxide was observed on top of the sample consisting mainly of Cr and trace amounts of Fe. 316Ti suffered from an intergranular corrosion attack after 6 months of exposure (see Fig. 3b). This attack progressed with increased severity as a function of exposure time. The corrosion products formed in the steel grain boundaries consisted mainly of a Cr-rich oxide. In addition, from the EDX map analysis it was confirmed that no sign of any chlorine species was detected throughout the sample. Below the metal/oxide surface, a roughly 150 μm thick Cr-depleted region had been formed throughout the sample (See Fig. 3e).

Fig. 4a and b show the cross-sections of the SX samples exposed for 6 and 12 months. Similar features were observed for both samples, and thus, chemical analysis via EDX mapping is only shown for the sample exposed for 12 months. A homogenous deposit layer was observed on both samples and consisted mainly of Ca, S, O, and traces of Na. In addition, minor traces of Cl were detected in the inner regions of the deposit. The thickness of the deposit was in the order of 60 – 150 μm for 12 and 6 months, respectively. SX formed an adherent outer corrosion product layer composed mainly of a Fe-rich oxide (see Fig. 4c). The outer oxide layer became less adherent with time, which is displayed in Fig. 4b, where large cracks after 12 months of exposure were observed. As with 316Ti, intergranular attacks were noticeable after 6 months of exposure and became more severe with time (compare Fig. 4a with 4b). The internal oxidation at the metal/oxide interphase consisted mainly of a Cr and Si-rich oxide and was propagating via grain boundaries through the material. After 12 months of exposure, at roughly 60 μm below the metal/oxide interphase, the chemical composition in the grain boundary

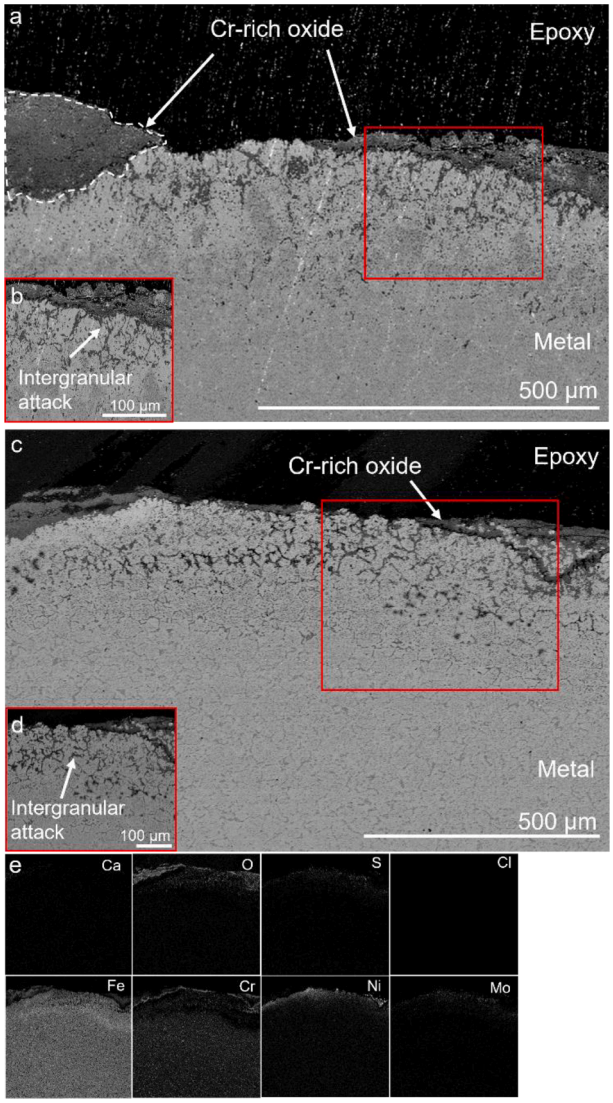

Fig. 3. SEM BSE cross-section image of 316Ti (a) 6 months of exposure. (b) Insert of intergranular attack after 6 months. (c) 12 months of exposure. (d) Insert of intergranular attack after 12 months. (e) EDX mapping of (c).

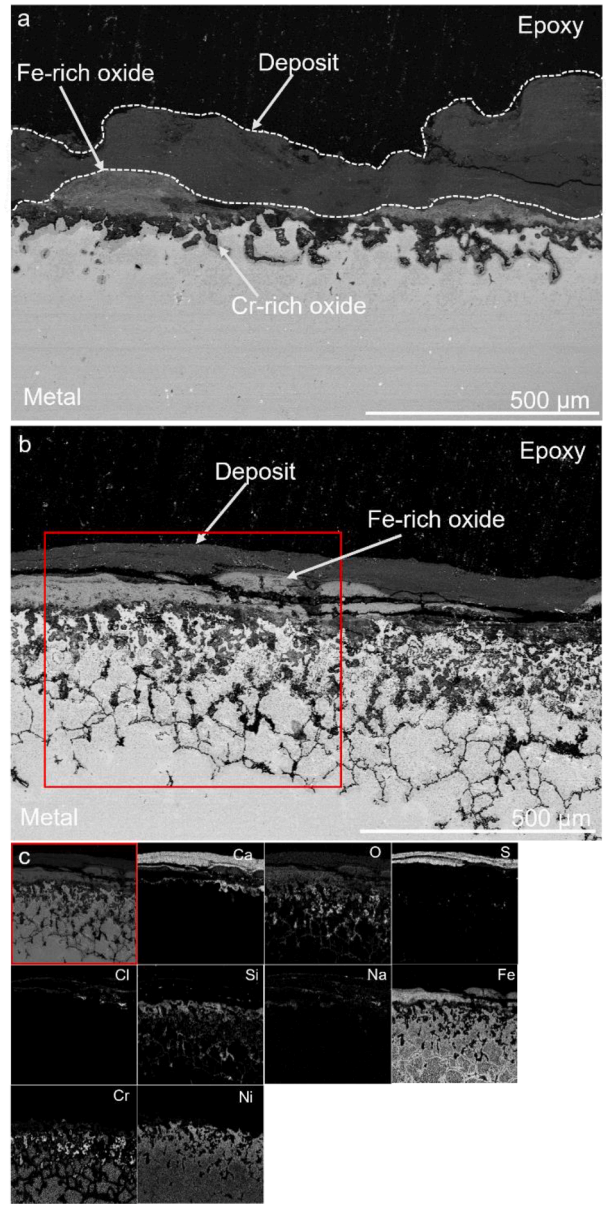

Fig. 4. SEM BSE cross-section image of SX after (a) 6 months of exposure. (b) 12 months of exposure. (c) EDX mapping of SX from the highlighted area in (b).

region changed, and a Cr-depleted region were obtained with the formation of Si-rich oxide in the grain boundary together with Fe-enrichments at the border of the grain boundaries (see Fig. 4c).

3.2.2. Ni-base alloy San69

Fig. 5a shows the cross-section image of the San69 sample after 6 months of exposure. An approximately 50 μm thick deposit layer was observed containing mainly S, Ca, and O with traces of P and Mg (see Fig. 5b). No significant amount of deposit was identified in the formed oxide scale. A Ni-rich oxide was formed underneath the deposited layer, and at the metal/oxide interphase, an oxide containing a high amount of Cr was observed. In addition, a Cr-rich oxide was also detected further into the metal as an internal oxidation region approximately 80 μm below the corrosion product layer. This feature is presumably a 3D effect of this 2D cross-section imaging. The EDX mapping shows that the metal is mainly depleted of Cr, while nickel remains the main alloy element in the material matrix close to the corrosion front. The material loss measurement of San69 was negligible after 6 months of exposure. However, based on the SEM/EDX analysis, the internal corrosion attack can be seen up to 0.3 mm into the metal.

3.2.3. FeCrAl alloys

A SEM cross-sectional view of the EF100 sample exposed for 6 months is shown in Fig. 6a. An approximately 250 μm thick deposit was observed, consisting primarily of S, Ca, and O. Beneath the deposited layer, an approximately 100 μm thick iron oxide had formed. The oxide contained small cracks and displayed void formations, whereas it was difficult to distinguish regions of inward and outward oxide layer formation. A roughly 10 μm Al/Cr-rich thin oxide layer was detected across the metal/oxide interphase (see Fig. 6b). The SEM analysis revealed no indications of internal oxidation for this material. However, a nitridation zone could be seen below the metal/oxide interphase. The thickness of the region varied greatly (between 0 and 200 μm) and was observed in a patch-wise fashion throughout the cross-section of the sample.

EF100 displayed similar features after 6 and 12 months of exposure (compare Fig. 6a and Fig. 7a). However, for the sample exposed for 12 months, most of the deposited layer had spalled off. This may however be an effect of sample outtake and subsequent sample preparation for post-analysis measurements. A Fe-rich oxide was observed (about 600 μm in thickness) containing voids and cracks as well as traces of Cr and Al (see Fig. 7a and c). The nitridation zone had also grown larger compared to after 6 months of exposure (about 400 μm in thickness) and was observed throughout the cross-section of the sample in a homogenous fashion. The EDX analysis confirmed that the dark particles shown in the nitridation zone consisted of Alumina Nitrides (AlN) precipitates embedded in a Fe-rich alloy matrix (see Fig. 7b). The observed microstructures and corrosion attacks agree well with the measured material losses. The material loss for EF100 after 6 and 12 months was 0.13 and 0.19 mm, respectively. The SEM/EDX analysis after 12 months of exposure also shows that a region (roughly 125 μm thick) depleted in Cr was detected at the nitridation/metal interphase (see Fig. 7c). This Cr-depletion zone was homogenous and observed throughout the sample. No Cl was detected in the corrosion front or the deposit. Regardless of exposure time, the sample was covered by corrosion products and, for the 6-month exposed sample, deposit. Thus, it is suggested that the material loss is primarily driven by a corrosion process rather than erosion.

EF101 displayed similar features as EF100 after 6 months of exposure (see Fig. 8a). The EDX map analysis of EF101 shows that a thin deposit layer (about 25 μm in thickness) had formed above the oxide layer containing large amounts of Ca (see Fig. 8c). The oxide scale was composed of a Fe-rich oxide containing cracks and voids (see Fig. 8b). Traces of a Cr rich oxide were also observed but to a lower extent. Below the Fe-rich oxide a roughly 8 μm thin Al-rich oxide layer was observed. In addition, below the metal/oxide interface, a Cr-depleted zone of approximately 100 μm was seen. Compared to EF100, the EF101 sample exhibited a more pronounced nitridation zone. The thickness of the nitridation zones was 450 μm and 200 μm for EF101 and EF100, respectively, after 6 months. For EF101, the SEM analysis revealed no or small amounts of deposit components. In addition, no traces of chlorine-containing species were observed in the cross-section (see Fig. 8c).

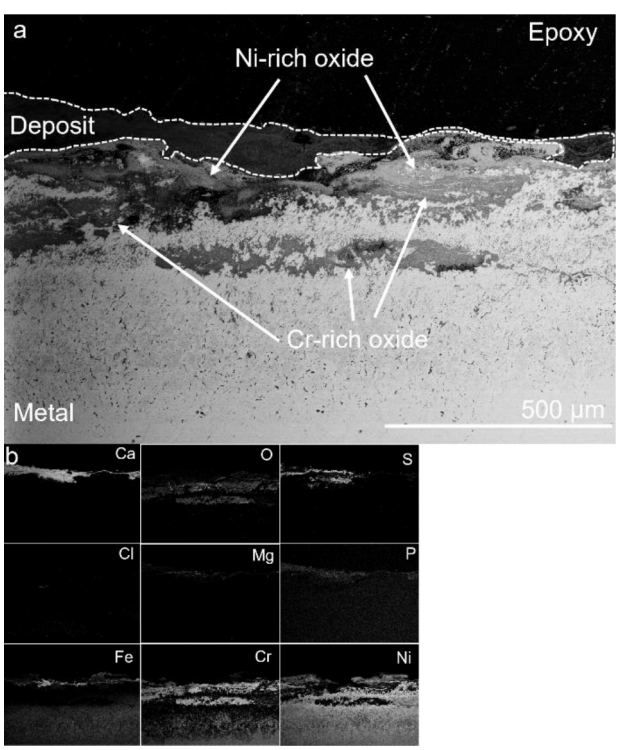

Fig. 5. SEM BSE cross-section image of San69 (a) after 6 months of exposure. (b) EDX mapping of (a).

4. Discussion

The aim of this study was to evaluate the performance of two newly developed FeCrAl alloys exposed within the FBHE of a waste-fired CFB boiler in Sweden for 6 and 12 months. The material temperature was estimated to 500–520 °C, and the fuel composition consisted of a mixture of industrial and household waste. In addition, several other materials were investigated to compare the achieving results. The materials investigated were the austenitic stainless steels 316Ti and SX, a Ni-base alloy Sanicro 69, and two FeCrAl alloys Kanthal® EF100 and EF101.

316Ti presented the highest material loss after 6 and 12 months of exposure compared to the other materials (see Fig. 2). The material was subjected to a large degree of intergranular corrosion and the severity of the corrosion attack was increased as a function of time exposed to the present environment (see Fig. 3). In mild environments, austenitic stainless steels, such as, e.g., 347H, 304L, and 316Ti, are expected to form a chromium-rich and protective oxide [23]. In environments rich in alkali chlorides, this group of materials is readily attacked by both alkali and chlorine forming alkali chromates and metal with a corrosion product layer often consisting of an outward-growing hematite (Fe_2O_3) and an inward-growing (mixed) spinel oxide layer (Me_3O_4) [24]. In this study, only the inward-growing spinel oxide (rich in Cr and Ni, see Fig. 3, remains on the sample, whereas the outward-growing hematite as well as the deposited layer, have been lost. It is expected that the presence of alkali in the environment has destroyed the protective properties of the initial chromium-rich oxide [13,23]. Furthermore, an intergranular attack in the form of a steel grain boundary (GB) attack can be seen. In a recent study, the attack is associated with small levels of chlorine in

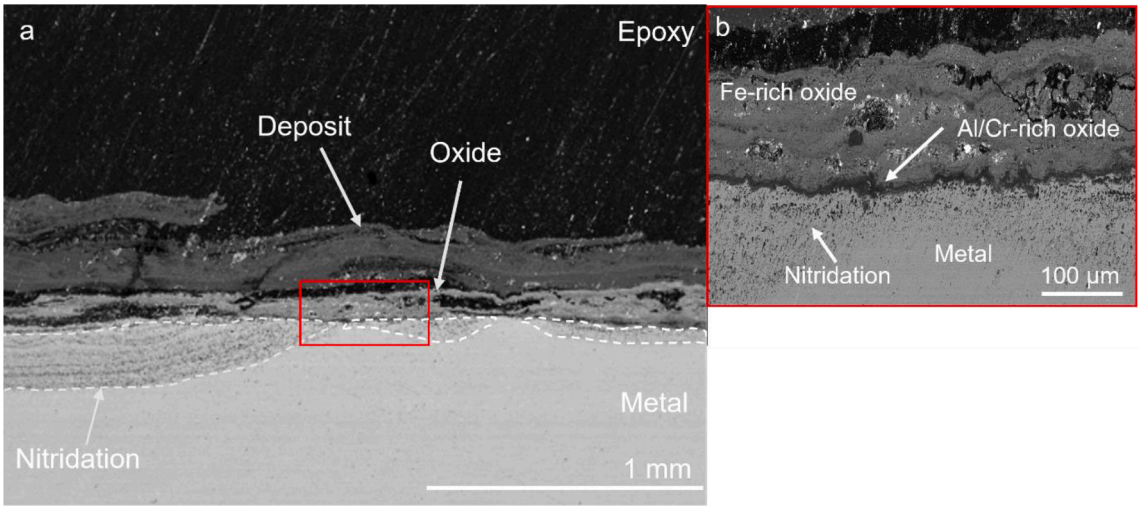

Fig. 6. (a) SEM BSE cross-section image of EF100 after 6 months of exposure. (b) Higher magnification of the marked area in (a).

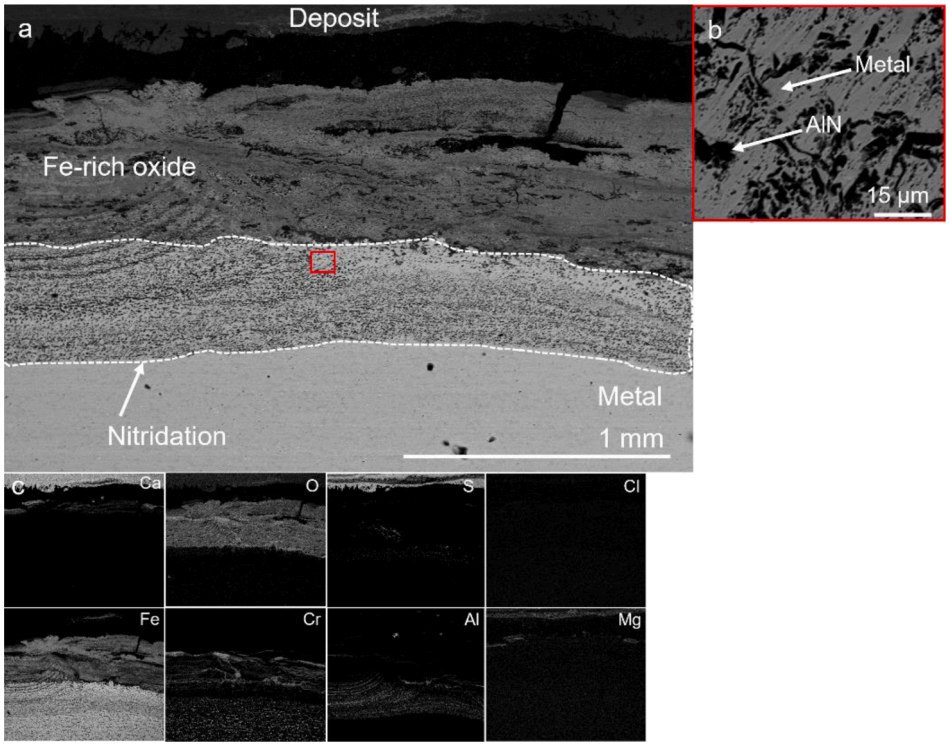

Fig. 7. SEM BSE cross-section image of EF100 (a) after 12 months of exposure.(b) Higher magnification of the marked area in (a). (c) EDX mapping of (a).

the GB's [25]. In the article referred to, chlorine is suggested to increase the diffusivity at the GB's and thereby cause accelerated corrosion. This type of behavior is expected to be detrimental to the material over time, either by continuing the attack to spread laterally or by losing whole steel grains, as the attack decreases the mechanical stability of the material. In order to conclude that the corrosion attack in the GB's in this study is driven by chlorine, more advanced microscopy is needed (e.g., TEM).

The austenitic alloy SX exhibited a qualitatively similar corrosion attack as 316Ti. However, the material loss was significantly lower. Compared to 316Ti, the SX alloy contains about twice the amount of Ni and about five times the amount of Si (see Table 1). It has been shown earlier that alloying with Ni usually results in a lower corrosion rate in aggressive corrosive environments [22]. Persdotter et al. have proposed that the increase of Ni in Fe-based alloys primarily decreases the corrosion rate in the secondary protection regime at 600 °C, i.e., after breakaway corrosion has occurred [24]. The low material loss for the Ni-base alloy San69 further suggests that the addition of nickel in this environment reduces the rate of material degradation, based on the 6-month sample. In a previous study, small material losses were observed for Ni-rich austenitic steel (32 wt% Ni) situated in the loop seal of a biomass boiler for 12 months of exposure, which further suggests that this material may exhibit good protective properties in the present environment even after 12 months of exposure [14]. The presence of Si in high-temperature materials has also been reported to have a beneficial effect on corrosion protection [26,27]. However, it is not fully understood within this study how silicon affects corrosion protection properties in SX.

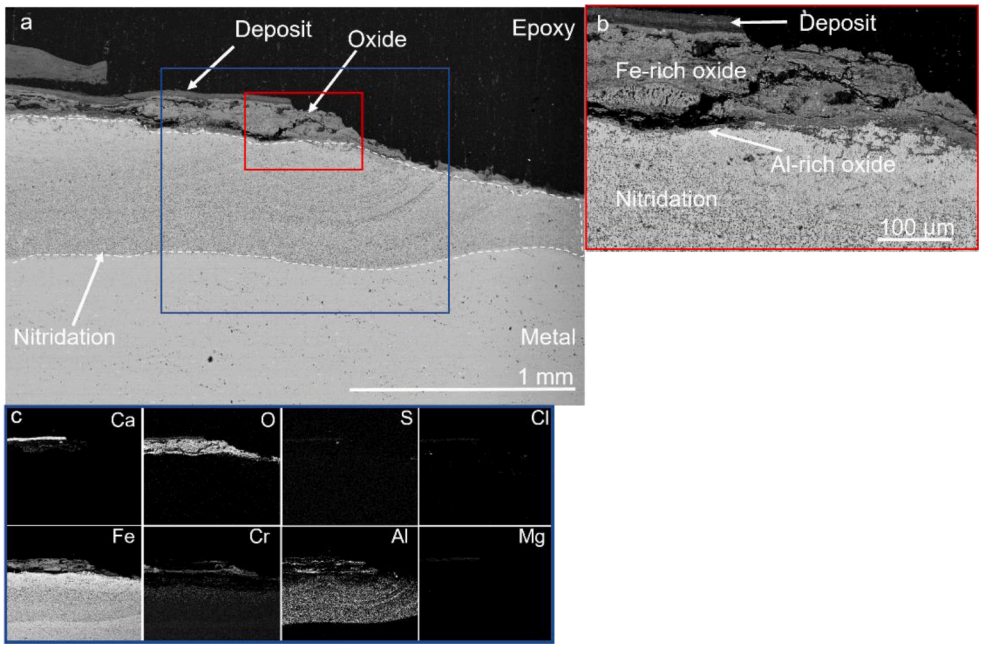

Fig. 8. SEM BSE cross-section image of (a) EF101 after 6 months of exposure. (b) Higher magnification of the small marked red area in (a). (c) EDX mapping of the sizeable, marked area in (a). (For interpretation of the references to colour in this figure legend, the reader is referred to the web version of this article.)

In the case of the FeCrAl alloys, EF101 (which contains 1.3 wt% Si), obtained a material loss that was less compared to the corresponding EF100 sample after 6 months of exposure (see Fig. 2). Eklund et al. studied the effect of silicon and Cr addition on the corrosion resistance of FeCrAl model alloys positioned in the convection pass of a waste fired boiler. They observed a drastic decrease in the material loss for FeCrAl model alloys when adding 2 wt% Si at a material temperature of 600 °C exposed for 672 h. They acknowledged that the addition of Si significantly improved the secondary protection layer of the alloy by reducing the iron oxide growth rate in aggressive corrosive environments containing alkali chlorides [19]. These results align well with a previous laboratory study where a decrease in corrosion rate was observed with increased Si-content for FeCrAls in an environment containing oxygen, water vapour, and KCl at 600 °C [19]. In this study, a positive effect of Si alloying was also observed when comparing the material loss of EF101 to EF100 after 6 months of exposure, suggesting that Si may play an important role in material degradation mechanisms.

For both FeCrAl alloys, after 6 months of exposure, the formation of a nitridation zone was observed. This observation aligns well with previous studies, which have also reported the formation of nitridation zone in nitrogen-containing environments of FeCrAl alloys [28].

The EF101 obtained a thicker nitridation zone after 6 months of exposure compared to EF100 (compare Fig. 6a and 8a). The resistance towards nitridation can be due to several factors, such as the concentration of Cr in the alloy, the integrity of the alumina scale including micro defects in the oxide, which allows the nitrogen to diffuse through the deposit and oxide scale. The nitridation is, from a corrosion point of view, not desirable as the aluminum in the alloy is tied up locally in the formation of AlN rather than forming a protective alumina scale. Despite this, the newly developed FeCrAl alloys showed good material performance in this environment, and the material losses of the investigated materials were rather low.

Lastly, the FBHE localized in the loop seal region of a CFB boiler may be experiencing both corrosive and erosive forces. Based on earlier studies, the material loss of the FBHE is explained by both these degradative forces, singularly or in combination [14,29]. A previous study in the present boiler shows that this area of the boiler has experienced high material wastage of the FBHE, up to about 4 mm/year, due to high erosive forces [29]. The FBHE is surrounded by fluidized bed material, and thus erosion is expected on the sample. However, the erosive influence of the attack seems less aggressive in this study compared to the previous one. In the current study, the samples were generally covered by both corrosion products and deposits, indicating that material loss is mainly derived through a corrosion process rather than erosion. Despite this, samples were experiencing spallation and poor adherence of deposit and corrosion product layers. However, this may be the result of sample outtake and sample preparation rather than removal due to erosive forces, and further investigations are needed to increase the understanding of how the interplay between erosion and corrosion may have synergetic effects in this part of the boiler.

5. Concluding remarks

- Of the five alloys exposed for 6 and 12 months clamped on the FBHE in the loop seal region of a waste-fired boiler, minor material degradation was observed for all the materials, except 316Ti, owing to a non-aggressive corrosive environment together with low erosive properties of the bed material in the loop seal region.
- The FeCrAl alloys (Kanthal® EF100 and EF101) performed well in the present environment, achieving material losses that were lower than for 316Ti and on par with the commercialized austenitic steel SX. Both FeCrAl materials were subjected to nitridation below the metal/oxide interphase and the formation of an outer Fe-rich oxide. No significant difference in material loss or corrosion features was observed between EF100 & EF101.
- The austenitic steels 316Ti and SX were both subjected to intergranular corrosion. However, 316Ti exhibited much more severe material loss.
- For the Ni-base alloy San69, negligible material loss was reported after 6 months of exposure. An internal Cr-rich oxide formation defined the corrosion attack with no traces of significant intergranular corrosion.

Funding

This work was funded by the Swedish Energy Agency and is associated with KME (Consortium of materials technology for thermal energy processes).

CRediT authorship contribution statement

Hampus Lindmark: Conceptualization, Methodology, Investigation, Data curation, Validation, Visualization, Writing – original draft. **Julien Phother:** Resources, Writing – review & editing. **Maria Dolores Paz Olausson:** Resources, Writing – review & editing. **Johanna Nockert:** Resources, Writing – review & editing. **Fredrik Lind:** Resources, Writing – review & editing. **Anna Jonasson:** Resources, Writing – review & editing. **Vesna Barišić:** Resources, Writing – review & editing. **Kyösti Vänskä:** Resources, Writing – review & editing. **Laura Rioja-Monllor:** Resources, Writing – review & editing. **Jesper Liske:** Conceptualization, Writing – review & editing, Project administration, Funding acquisition, Supervision.

Declaration of Competing Interest

The authors declare that they have no known competing financial interests or personal relationships that could have appeared to influence the work reported in this paper.

Data availability

Data will be made available on request.

Acknowledgment

The authors would like to acknowledge two anonymous reviewers for their insightful comments that helped improve the quality of the manuscript. This paper has been part of a collaboration between Kanthal AB, Alleima AB, E.On Energy Infrastructure AB, Sumitomo SHI FW, and The High Temperature Corrosion Centre at Chalmers University of Technology. Each participant is highly acknowledged for their input and support.

References

[1] Ericsson K, Werner S. The introduction and expansion of biomass use in Swedish district heating systems. Biomass Bioenergy 2016;94:57–65.
[2] Ridjan I, Mathiesen BV, Connolly D. A review of biomass gasification technologies in Denmark and Sweden. 2013.
[3] Ranta T, Laihanen M, Karhunen A. Development of the bioenergy as a part of renewable energy in the Nordic Countries: A comparative analysis. J Sustainable Bioenergy Systems 2020;10(3):92–112.
[4] Amin NAS. Reducing CO2 emissions in biomass power plants using the incam model. 2016.
[5] Bankiewicz D, Vainikka P, Lindberg D, Frantsi A, Silvennoinen J, Yrjas P, et al. High temperature corrosion of boiler waterwalls induced by chlorides and bromides–Part 2: Lab-scale corrosion tests and thermodynamic equilibrium modeling of ash and gaseous species. Fuel 2012;94:240–50.
[6] Kinnunen H, Hedman M, Engblom M, Lindberg D, Uusitalo M, Enestam S, et al. The influence of flue gas temperature on lead chloride induced high temperature corrosion. Fuel 2017;196:241–51.
[7] Enestam S, Bankiewicz D, Tuiremo J, Mäkelä K, Hupa M. Are NaCl and KCl equally corrosive on superheater materials of steam boilers? Fuel 2013;104:294–306.
[8] Eklund J, Paz MD, Jönsson B, Liske J, Svensson JE, Jonsson T. Field exposure of FeCrAl model alloys in a waste-fired boiler at 600° C: The influence of Cr and Si on the corrosion behaviour. Mater Corros 2019;70(8):1476–85.
[9] Sharp W. Superheater corrosion in biomass boilers: Today's Science and Technology. Oak Ridge National Laboratory 2010;3.
[10] Jensen PA, Frandsen FJ, Hansen J, Dam-Johansen K, Henriksen N, Hörlyck S. SEM investigation of superheater deposits from biomass-fired boilers. Energy Fuel 2004;18(2):378–84.
[11] Michelsen HP, Frandsen F, Dam-Johansen K, Larsen OH. Deposition and high temperature corrosion in a 10 MW straw fired boiler. Fuel Process Technol 1998;54(1–3):95–108.
[12] Paz L, Jonsson T, Liske J, editors. Testing of new materials to combat superheater corrosion in a waste fired CFB boiler. 23rd International conference on Fluidized Bed Conversion; 2018.
[13] Jonsson T, Froitzheim J, Pettersson J, Svensson J-E, Johansson L-G, Halvarsson M. The influence of KCl on the corrosion of an austenitic stainless steel (304L) in oxidizing humid conditions at 600 C: a microstructural study. Oxid Met 2009;72(3):213–39.
[14] Nafari A, Nylund A. Field study on superheater tubes in the loop seal of a wood fired CFB plant. Mater Corros 2004;55(12):909–20.
[15] Norling R, Olefjord I. Erosion–corrosion of Fe-and Ni-based alloys at 550° C. Wear 2003;254(1–2):173–84.
[16] Rishel D, Pettit F, Birks N. Some principal mechanisms in the simultaneous erosion and corrosion attack of metals at high temperatures. Mater Sci Eng A 1991;143(1–2):197–211.
[17] Li N, Parker SS, Wood ES, Nelson AT. Oxide morphology of a FeCrAl alloy, kanthal APMT, following extended aging in air at 300° C to 600° C. Metall Mater Trans A 2018;49(7):2940–50.
[18] N. Israelsson High temperature oxidation and chlorination of FeCrAl alloys: Chalmers Tekniska Hogskola 2014 (Sweden).
[19] J. Eklund High Temperature Corrosion of FeCrAl Alloys in Biomass-And Waste-Fired Boilers-The Influence of Alloying Elements in Prediction and Mitigation of Corrosion in Harsh Environments: Chalmers Tekniska Hogskola 2020 (Sweden).
[20] Asokan V, Eklund J, Bigdeli S, Jonsson T. The influence of Si on the primary protection of lean FeCrAl model alloys in O2 and O2+ H2O at 600° C—A microstructural investigation. Corros Sci 2021;179:109155.
[21] Sand T, Edgren A, Geers C, Asokan V, Eklund J, Helander T, et al. Exploring the Effect of Silicon on the High Temperature Corrosion of Lean FeCrAl Alloys in Humid Air. Oxid Met 2021;95(3–4):221–38.
[22] Eklund J, Jönsson B, Persdotter A, Liske J, Svensson J-E, Jonsson T. The influence of silicon on the corrosion properties of FeCrAl model alloys in oxidizing environments at 600 C. Corros Sci 2018;144:266–76.
[23] Pettersson J, Asteman H, Svensson J-E, Johansson L-G. KCl induced corrosion of a 304-type austenitic stainless steel at 600 C; the role of potassium. Oxid Met 2005;64(1):23–41.
[24] Persdotter A, Eklund J, Liske J, Jonsson T. Beyond breakaway corrosion–Influence of chromium, nickel and aluminum on corrosion of iron-based alloys at 600° C. Corros Sci 2020;177:108961.
[25] Phother-Simon J, Hanif I, Liske J, Jonsson T. The influence of a KCl-rich environment on the corrosion attack of 304 L: 3D FIB/SEM and TEM investigations. Corros Sci 2021;183:109315.
[26] Jonsson T, Canovic S, Liu F, Asteman H, Svensson J-E, Johansson L-G, et al. Microstructural investigation of the effect of water vapour on the oxidation of alloy 353 MA in oxygen at 700 and 900 C. Mater High Temp 2005;22(3–4):231–43.
[27] Mao H-h, Qi X, Cao J, An L-c, Yang Y-t. Effect of Si on high temperature oxidation of 30Cr13 stainless steel. J Iron Steel Res Int 2017;24(5):561–8.
[28] Mortazavi A, Esmaily M, Geers C, Birbilis N, Svensson J-E, Halvarsson M, et al. Exploring failure modes of alumina scales on FeCrAl and FeNiCrAl alloys in a nitriding environment. Acta Mater 2020;201:131–46.
[29] Ekström A. Conditions of increased life time of superheaters in loop seals. Uppsala University; 2018 [Master thesis]. Available from:.